

A Numerical Experiment on Oscillatory Magnetic Reconnection in a Laboratory Plasma System Driven by Alternating Currents

SRIPAN MONDAL,¹ ABHISHEKH KUMAR SRIVASTAVA,² AND ERIC R. PRIEST³

¹*Department of Physics, Indian Institute of Technology (BHU), Varanasi-221005, India*

²*Department of Physics, Indian Institute of Technology (BHU), Varanasi-221005, India. Email:- asrivastava.app@itbhu.ac.in*

³*Mathematics Institute, St Andrews University, KY16 9SS, St Andrews, UK*

ABSTRACT

Using the open source MPI-AMRVAC framework, we study oscillatory reconnection in a laboratory plasma, which occurs when a magnetic null is perturbed by incoming fast magnetoacoustic waves driven by an alternating current. The magnetic null region collapses to first form a y -directed current sheet that later changes its orientation to the x -direction. The x -directed current sheet has smaller enhanced thermal pressure and out-of-plane current than the y -directed current sheet. The Hall effect produces an out-of-plane plasma flow that evolves with a time lag with respect to the enhanced thermal pressure and out-of-plane current density. Increasing the amplitude of the alternating current produces higher thermal pressure, out-of-plane current density, and out-of-plane plasma flow, while the first peaks of thermal pressure and out-of-plane current density occur earlier.

Keywords: Hall Magnetohydrodynamics; MHD Waves; Magnetic Reconnection; Laboratory Plasma

1. INTRODUCTION

Breaking and topological rearrangement of magnetic field lines, namely, magnetic reconnection, occurs in different plasma systems such as solar and space plasmas, planetary magnetospheres, and laboratory fusion plasmas (e.g., Yamada et al. 2010; Hesse & Cassak 2020; Nakamura et al. 2025). Such a process can result in the liberation of non-potential magnetic energy stored in the magnetic configurations and its transformation into heat, bulk kinetic energy of the plasma, and kinetic energy of charged particles (e.g., Goedbloed & Poedts 2004; Priest 2014). In principle, magnetic reconnection is a three-dimensional process, which can take place near the magnetic nulls, separators, or quasi-separators configured in various kinds of magnetic geometry (e.g., Pontin & Priest 2022). A two-dimensional description of magnetic reconnection requires a magnetic X-type geometry in which a magnetic null is located at the intersection of two separatrix curves (e.g., Pontin & Priest 2022). However, the formation of a sheet of high current density (namely, a current sheet) is an essential step towards the onset of magnetic reconnection irrespective of the geometry.

Investigations of magnetic reconnection have been carried out using observational data from the space satellites for both solar (e.g., Drake et al. 2025) and magnetospheric plasmas (e.g., Gershman et al. 2024). Several dedicated laboratory experiments such as MRX (Magnetic Reconnection Experiment) (e.g., Yamada et al. 2005, 2014, 2016) and TREX (e.g., Olson et al. 2016) have been set up to improve our understanding of reconnection in the laboratory. There are also laser-induced high energy density experiments of magnetic reconnection (e.g., Fox et al. 2011; Fiksel et al. 2014; Egedal 2021; Fox et al. 2022). In addition, there are experiments driven by pulsed-power platforms in which the plasma pressure is on the order of the magnetic pressure (e.g., Hare et al. 2017).

In parallel, numerical simulations play a significant role in enhancing the existing understanding of magnetic reconnection at disparate spatio-temporal scales (e.g., Pontin et al. 2024; Moreno-Insertis et al. 2025; Shay et al. 2025; Richter et al. 2025). Single-fluid magnetohydrodynamic (MHD) models are frequently used in two- or three-dimensional models. However, when ions and electrons are decoupled, a two-fluid prescription is preferable. If the length-scale of plasma dynamics is larger than the electron inertial length but smaller than the ion inertial length, corrections due to the Hall effect need to be incorporated into the MHD equations, which is the focus of this paper (e.g., Birn et al.

2001; Huba & Rudakov 2002; Huba 2003; Huba & Rudakov 2003; Knoll & Chacón 2006; Malakit et al. 2009; Stanier et al. 2017).

If the initiation is associated with MHD instabilities such as the resistive tearing mode or the ideal kink mode (e.g., Baty 2000; Browning et al. 2024), it is termed spontaneous reconnection. However, if the reconnection is caused by some external driving such as flux emerging from below the solar surface, erupting prominences or magnetoacoustic waves (e.g., Sakai et al. 1984; Vekstein 2017; Srivastava et al. 2019), it is regarded as externally driven reconnection. In laboratory plasma systems, most of the experiments have reconnection that is externally driven (e.g., Yamada et al. 1997; Hare et al. 2017).

Since various kinds of wave mode are ubiquitous in the solar corona, they can interact with nulls, separators or quasi-separators to initiate magnetic reconnection. This process, together with the possibility of reconnection driving waves, is referred to as a ‘Symbiosis of Waves and Reconnection (SWAR)’ (e.g., Mondal et al. 2024; Srivastava et al. 2025). At laboratory scales, such a process has been studied using an experiment in which an alternating current varying between 40 kA and 70 kA with a half-period of 400 μ s generates fast magnetoacoustic waves that converge towards a magnetic null. This results in the accumulation of current to form a current sheet that gradually thins in the presence of Hall currents and inverse currents (e.g., Frank & Savinov 2024).

In the solar corona, if a current sheet changes its orientation from, say, vertical to horizontal or vice-versa, it is termed oscillatory reconnection (e.g., Craig & McClymont 1991; McLaughlin et al. 2009; Thurgood et al. 2017; Karampelas et al. 2022). However, the periodicity of such an oscillation depends on the background plasma parameters rather than the details of the driver and can take place in a self-consistent manner even in the absence of continuous driving (e.g., Karampelas et al. 2023). Moreover, in a reconnection experiment in MRX, it has been found that, during an increase of current in the poloidal flux loops from 0 to 15 kA, a vertical current sheet is formed, which undergoes ‘Push’ reconnection. Then, during a decrease of the current, the sheet changes its orientation and undergoes ‘Pull’ reconnection (e.g., Yamada et al. 1997).

Here, we conduct a two-dimensional Hall-MHD simulation of such externally-driven oscillatory reconnection in a plasma system that is magnetically dominated. Our main aim is to examine how physical variables change with time during the collapse of a magnetic null due an alternating current flowing through wires close to the boundary of the simulation domain. In section 2, the numerical setup is presented along with the adopted numerical methods. In section 3, the scientific outcomes are demonstrated and discussed in detail. This is followed by a summary of the findings in the section 4.

2. SETUP FOR THE NUMERICAL EXPERIMENT

We consider a plasma system having a uniform number density (n_0) of 10^{13} cm^{-3} and a temperature (T_0) of 10^5 K, i.e., around 8.6 eV, which are similar to those used in the MRX setup while conducting a study of collisional magnetic reconnection in a low- β (i.e., magnetically dominated) plasma. The resulting Debye length ($\lambda_D = \sqrt{\epsilon_0 k_B T_0 / n_0 e^2}$) is estimated to be around 7×10^{-4} cm, while the electron inertial length ($d_e = \sqrt{\epsilon_0 m_e c^2 / n_0 e^2}$) and ion inertial length ($d_i = \sqrt{\epsilon_0 m_p c^2 / n_0 e^2}$) are 0.17 cm and 7.2 cm, respectively. Here, ϵ_0 , k_B , c , m_e and m_p are the permittivity of free space, Boltzmann constant, speed of light, electron mass and proton mass, respectively. We consider a two-dimensional simulation domain spanning over $[-7.5d_i, 7.5d_i]$, (i.e., $[-54$ cm, 54 cm]) in both the x - and y -directions.

We place four straight wires each having length (L) of 360 cm, extending from $z = -180$ cm to $z = +180$ cm in the z -direction at the following locations: $(x_1, y_1) = [0$ cm, -216 cm], $(x_2, y_2) = [0$ cm, $+216$ cm], $(x_3, y_3) = [-216$ cm, 0 cm] and $(x_4, y_4) = [+216$ cm, 0 cm]. Direct currents of amplitude $I_{dc} = 72$ kA flow through each wire in the positive z -direction. The resulting magnetic field possesses a magnetic null patch at the middle of the simulation domain in the $z = 0$ plane (see Fig. 1(a)). If we define

$$r_i^2 = (x - x_i)^2 + (y - y_i)^2 \quad (1)$$

for $i = 1, 2, 3, 4, 5, 6$, then the x -component of the magnetic field in the $z = 0$ plane can be written as–

$$B_{0x} = - \sum_{i=1}^2 \frac{I_{dc} L (y - y_i)}{r_i^2 \times \sqrt{r_i^2 + L^2/4}} + \sum_{i=3}^4 \frac{I_{dc} L (y - y_i)}{r_i^2 \times \sqrt{r_i^2 + L^2/4}}, \quad (2)$$

while the y -component in the same plane is

$$B_{0y} = \sum_{i=1}^2 \frac{I_{dc} L (x - x_i)}{r_i^2 \times \sqrt{r_i^2 + L^2/4}} - \sum_{i=3}^4 \frac{I_{dc} L (x - x_i)}{r_i^2 \times \sqrt{r_i^2 + L^2/4}}. \quad (3)$$

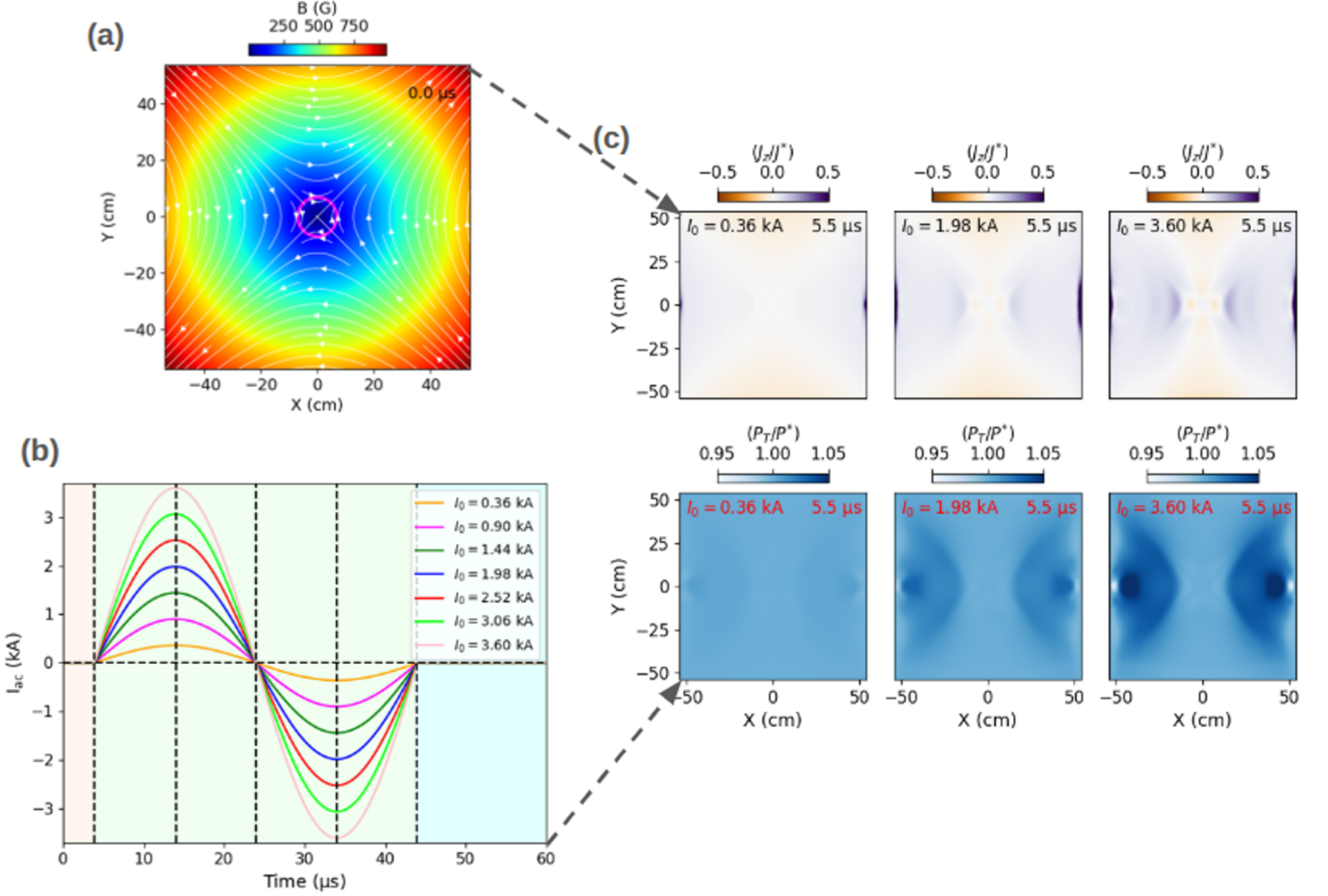


Figure 1. (a) The initial magnetic field configuration, in which the $\beta = 1$ curve where the thermal (P_T) and magnetic (P_M) pressure are equal is denoted by a magenta circle. (b) The variation with time of the alternating currents of different amplitude imposed at the left and right side boundaries; vertical dashed lines correspond to times of 3.9 μ s, 13.9 μ s, 24 μ s, 34 μ s and 44 μ s. (c) The perturbations in magnetic field and plasma as wave-like fronts seen in the z -component of current density (J_z) (top row) and P_T (bottom row) at 5.5 μ s for three different amplitudes of the alternating current. The inward propagation of the initial wave-like perturbations from 0 to 7.6 μ s is shown in Fig1c.mp4 (Multimedia available online).

Since, these wires are far away from the boundaries of the simulation domain, the resulting magnetic field is in quasi-static equilibrium in the presence of a uniform density and temperature, if it is not subjected to any other perturbations.

We place two more straight z -directed wires of length $L_1 = 3.6$ cm, along which alternating currents flow at the following locations: $(x_5, y_5) = [-57.6 \text{ cm}, 0 \text{ cm}]$, and $(x_6, y_6) = [57.6 \text{ cm}, 0 \text{ cm}]$. The periodicity and phase of the alternating currents flowing through them are the same (see Fig. 1(b)) and have the form

$$I_{ac} = I_0 f(t), \quad (4)$$

where

$$f(t) = \begin{cases} 0 & \text{when } t \leq t_1; \\ \sin\left(\frac{2\pi(t-t_1)}{T}\right) & \text{when } t_1 \leq t \leq t_2; \\ 0 & \text{when } t > t_2, \end{cases} \quad (5)$$

where $t_1 = 4$ μ s, $t_2 = 44$ μ s and $T = 40$ μ s. We vary the amplitude I_0 from 0.36 kA to 3.60 kA to see how it affects the dynamics of the reconnection. The alternating currents generate a time-varying magnetic field given by

$$b_x = \frac{I_{ac} L_1 (y - y_5)}{r_5^2 \times \sqrt{r_5^2 + L_1^2/4}} + \frac{I_{ac} L_1 (y - y_6)}{r_6^2 \times \sqrt{r_6^2 + L_1^2/4}}, \quad (6)$$

$$b_y = -\frac{I_{ac}L_1(x-x_5)}{r_5^2 \times \sqrt{r_5^2 + L_1^2/4}} - \frac{I_{ac}L_1(x-x_6)}{r_6^2 \times \sqrt{r_6^2 + L_1^2/4}}. \quad (7)$$

We discretize the simulation domain using a resolution of 160×160 initially, which is then subjected to one level of adaptive mesh refinement to have an effective maximum resolution of 320×320 with the smallest cell size being 0.34 cm. Since, this smallest cell size is much smaller than the ion inertial length of 7.2 cm, the Hall effect decouples the ions and electrons and is well treated in our simulation. The smallest cell size is nearly twice the electron inertial length of 0.17 cm, but a full kinetic simulation would treat the electron behaviour better. Thus, we solve the following dimensionless Hall-MHD equations to simulate the magneto-plasma dynamics using open-source MPI-AMRVAC (e.g., Keppens et al. 2023):

$$\frac{\partial \rho}{\partial t} + \vec{\nabla} \cdot (\rho \vec{V}) = 0, \quad (8)$$

$$\frac{\partial}{\partial t}(\rho \vec{V}) + \vec{\nabla} \cdot [\rho \vec{V} \vec{V} + P_{tot} \vec{I} - \vec{B} \vec{B}] = 0, \quad (9)$$

$$\begin{aligned} \frac{\partial e}{\partial t} + \vec{\nabla} \cdot (e \vec{V} + P_{tot} \vec{V} - \vec{B} \vec{B} \cdot \vec{V}) + \\ \vec{\nabla} \cdot \left(\frac{\eta_H}{\rho} [(\vec{J} \cdot \vec{B}) \vec{B} - (\vec{B} \cdot \vec{B}) \vec{J}] \right) = 0, \end{aligned} \quad (10)$$

$$\frac{\partial \vec{B}}{\partial t} + \vec{\nabla} \cdot \left(\vec{V} \vec{B} - \vec{B} \vec{V} + \frac{\eta_H}{\rho} (\vec{B} \vec{J} - \vec{J} \vec{B}) \right) = 0, \quad (11)$$

where

$$P_{tot} = P_T + \frac{B^2}{2}, \quad e = \frac{P_T}{\gamma - 1} + \frac{1}{2} \rho V^2 + \frac{B^2}{2} \quad (12)$$

and

$$\vec{J} = \vec{\nabla} \times \vec{B}, \quad \vec{\nabla} \cdot \vec{B} = 0. \quad (13)$$

Here, $\eta_H = \rho/(n_e e)$, and the dimensionless value of η_H is derived from a normalized background density (e.g., Leroy & Keppens 2017). So, since the normalized background density in the present case is 1, the (dimensionless) value of η_H to be 1. We do not include a physical resistivity in the simulation.

Since Eqs. (8)-(13) are solved numerically, the variables have been made dimensionless by dividing the dimensional values by characteristic values. For example, the normalising length L^* is here the ion inertial length (7.2 cm). The corresponding temperature T^* and number density n^* are taken to be 10^5 K and 10^{13} cm $^{-3}$, respectively, whereas the density $\rho^* = 1.4n^*m_H$ is 2.34×10^{-11} g cm $^{-3}$, in terms of the hydrogen mass (m_H). The thermal pressure $P^* = 2.3n^*k_B T^*$ is 317.5 dyne cm $^{-2}$, while the other variables are magnetic field $B^* = \sqrt{4\pi P^*} = 63$ G, velocity $V^* = B^*/(\sqrt{4\pi\rho^*}) = 3.68 \times 10^6$ cm s $^{-1}$ and time $t^* = L^*/V^* = 2$ μ s.

Temporal integration is carried out using a ‘‘two-step’’ method, and the ‘‘Harten-Lax-van Leer (HLL)’’ Riemann solver (e.g., Harten 1983) is utilized to estimate the flux at cell interfaces. A second-order symmetric total variation diminishing limiter, namely ‘‘vanleer’’ (e.g., van Leer 1979) is used to suppress spurious numerical oscillations. Thermal pressure and density are fixed at their initial values at all four boundaries. On the side boundaries, the x -component of velocity is assumed to be antisymmetric, while the other two components are taken to be symmetric. On the top and bottom boundaries, the y -component of velocity is assumed to be antisymmetric with the other two components being symmetric. This ensures that the normal velocity vanishes at all four boundaries, which therefore reflect the plasma flows. Furthermore, we do not introduce any damping layers to damp the reflections. Hence, the boundary effects play a role in the dynamics under consideration, especially, in the absence of external driving. The imposed boundary conditions for the other variables except the magnetic field are similar to those considered previously (e.g., Karampelas et al. 2022).

3. RESULTS

Since the wires carrying the alternating currents are placed very close to the left and right side boundaries, such currents generate magnetic field perturbations, which then propagate inward into the simulation domain as fast magnetoacoustic waves and disturb the quasi-stable equilibrium. The waves can be modeled as perturbations in the

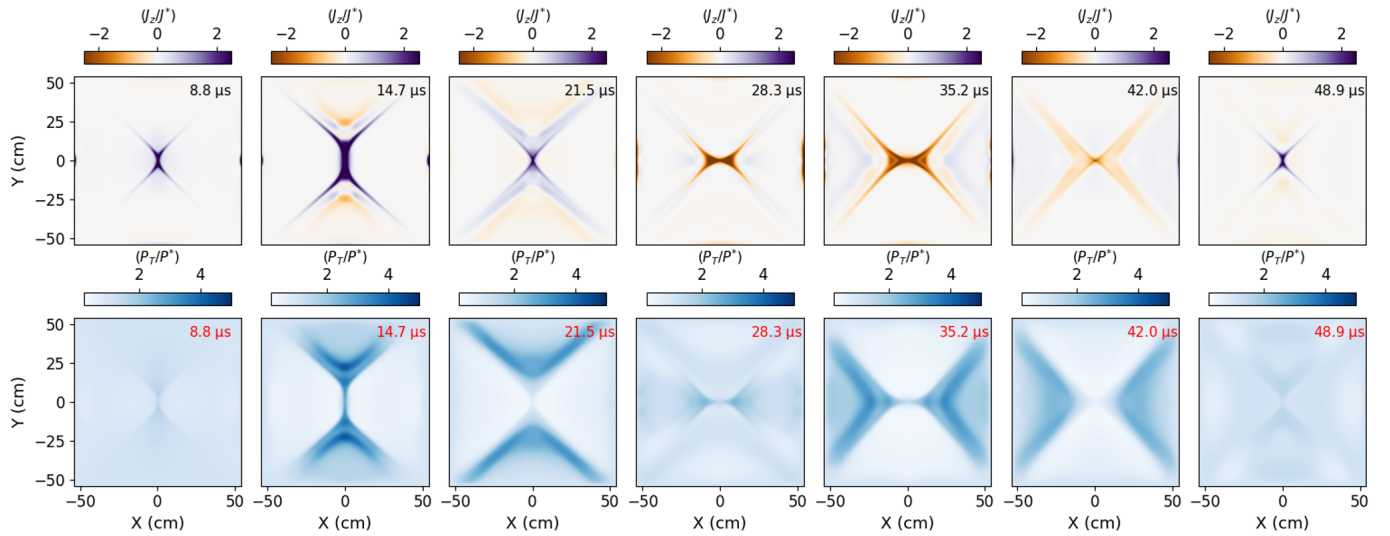


Figure 2. Variation with time of J_z (top row) and P_T (bottom row) for an imposed alternating current having an amplitude of 1.98 kA. J_z changes both its magnitude and direction, while the current sheet changes its orientation and back again. The final column shows the continuation of the oscillation after the driver has been switched off. The changes in J_z and P_T from 7.8 to 60 μ s are shown in Fig2.mp4 (Multimedia available online).

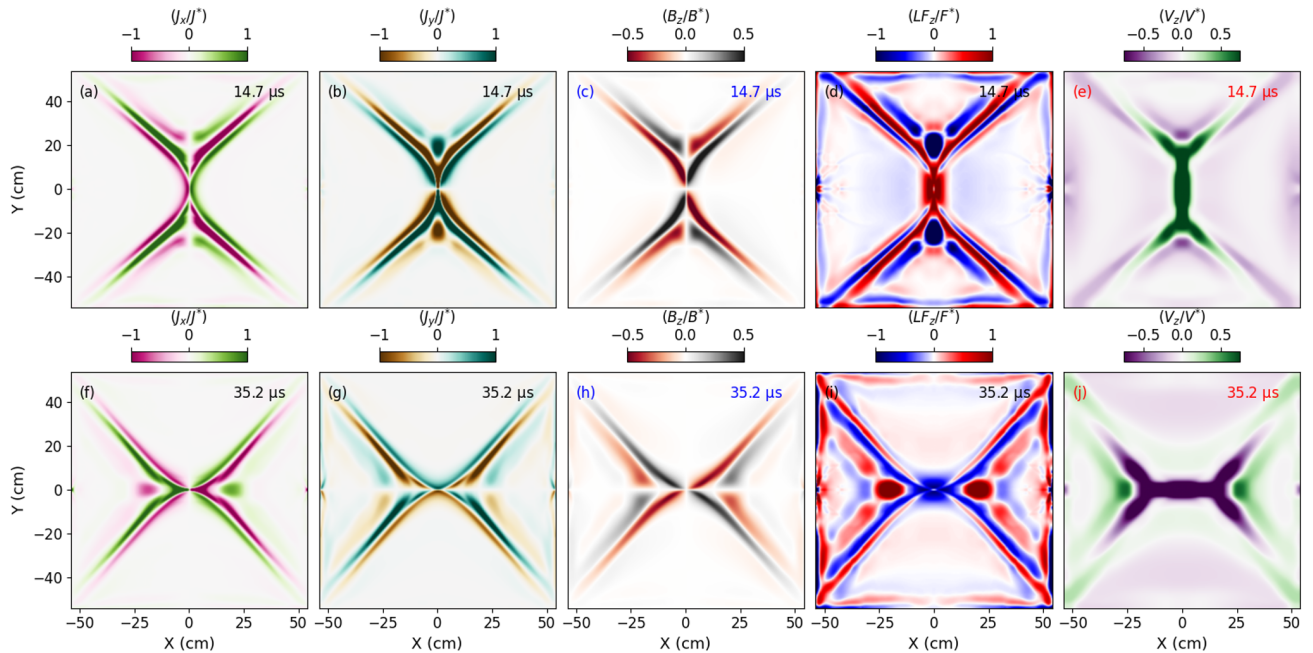


Figure 3. Spatial distribution of the in-plane current density components (J_x (first column) and J_y (second column)), out-of-plane magnetic field (B_z) (third column), out-of-plane Lorentz force (LF_z) (fourth column), and out-of-plane plasma flow (V_z) (fifth column) at 14.7 (top row) and 35.2 μ s (bottom row), when the imposed alternating current amplitude is 1.98 kA. The evolutions of J_x , J_y , B_z , LF_z , and V_z from 7.8 to 60 μ s are shown in Fig3.mp4 (Multimedia available online).

background magnetic field denoted via out-of-plane current density (say, J_z) and in the background plasma conditions such as in thermal pressure (P_T) (see Fig. 1(c) (Multimedia available online)). The waves are found to reach the magnetic null around 6.5 to 6.8 μ s after starting their propagation at 4 μ s from the alternating current carrying wires giving a propagation speed of 207 to 230 km s⁻¹. The amplitude of the perturbation increases with the amplitude of the driving alternating current (see Fig. 1(c)). Approaching fast magnetoacoustic waves cause the magnetic null point to collapse and form a current concentration at the null location and along the separatrices. In the following

subsection, we discuss the evolution in J_z and P_T with an alternating current of amplitude $I_0 = 1.98$ kA, determine the role of Hall effects on the dynamics, and further demonstrate the oscillation in the out-of-plane electric field.

3.1. Morphological Overview and Electric Field Oscillations for a Particular I_0

Due to the resulting unbalanced Lorentz force, the magnetic null eventually forms a y -directed current sheet with a strong current (J_z) directed out of the plane. The magnitude of J_z at first increases before beginning to decrease around $21 \mu\text{s}$ (see Fig. 2 (Multimedia available online)). From $24 \mu\text{s}$ to $44 \mu\text{s}$, the orientation of the current sheet changes to horizontal (i.e., the x -direction) along with a reversal of the direction of J_z . Such a change in the orientation of the current sheet is a manifestation of oscillatory reconnection. Comparatively weaker inverse J_z profiles are evident in the outflow regions at $14.7 \mu\text{s}$ and $35.2 \mu\text{s}$, associated with strong reconnection outflows. Moreover, even though the driving alternating current is switched off around $44 \mu\text{s}$, the cycle of current accumulation and reversal continues for some time (see right-most column of top row of Fig. 2). Such a persistence of oscillatory reconnection has previously been discussed (e.g., Craig & McClymont 1991; McLaughlin et al. 2009; Karampelas et al. 2022, 2023) and can occur also in the absence of a Hall term.

As discussed above, changes in J_z with time can give us an indication of how the magnetic topology changes in time. P_T increases within the current sheet structure and also along the separatrices with increasing J_z (see Fig. 2), as well as in the outflow regions. P_T decreases within the current sheet and along the separatrices when J_z decreases. However, a higher value of P_T persists in the outflow regions at farthest distances from magnetic Y-points and separatrices (see third and sixth column of bottom row of Fig. 2) most likely due to the combined effect of resistive heating and presence of Hall term. At later stages, after $44 \mu\text{s}$, P_T decreases almost to its initial value, which is similar to purely resistive behaviour.

To understand the role of the Hall effect, we consider the spatial distributions of in-plane currents (J_x and J_y) and out-of-plane magnetic field (B_z) (see Fig. 3 (Multimedia available online)), which vanish in resistive MHD but are a common feature of Hall-current models (e.g., Huba & Rudakov 2002; Huba 2003). Unlike J_z , the in-plane currents exist not within the current sheet but at its outer peripheries. In addition to the accumulation of in-plane currents along the separatrices, inverse J_x and J_y are present in the outflow region at $14.7 \mu\text{s}$ and $35.2 \mu\text{s}$, respectively (see Figs. 3(a) and (g)). Moreover, when a y -directed current sheet is present, there are localized peaks in $|J_y|$ along the outflow regions at $14.7 \mu\text{s}$ (see green and orange dotted structures in Fig. 3(b)). Similarly, for an x -directed current sheet, there are localized peaks in $|J_x|$ along the $y = 0$ line in the outflow regions at $35.2 \mu\text{s}$ (see green and magenta dotted structures in Fig. 3(f)). These additional features are associated with the presence of inverse J_z in the outflow regions (Frank & Savinov 2024).

The Hall current profile produces a quadrupolar configuration for B_z near the diffusion region, typical of Hall effects (e.g., Huba & Rudakov 2002; Huba 2003; Huba & Rudakov 2003; Shay et al. 2001; Uzdensky & Kulsrud 2006; Drake et al. 2008). Moreover, at times $14.7 \mu\text{s}$ and $35.2 \mu\text{s}$, a more complex nested B_z is found. Apart from the quadrupolar field concentrated along the magnetic separatrices, another set of oppositely oriented quadrupolar magnetic fields appears in the outflow regions in association with the inverse Hall currents (see Figs. 3(c), (h)). Therefore, the variation of this inverse B_z with x in the outflow regions near the peaks in $|J_y|$ possesses a high gradient as it reverses direction over a short distance across the peaks in $|J_y|$ (see Figs. 3(b)-(c)). Similarly, across the peaks in $|J_x|$, there are high gradients of inverse B_z along the y -direction (see Figs. 3(f), (h)).

In pure 2D MHD simulations in the xy -plane without any guide field, the Lorentz force will only have x - and y -components. However, the presence of in-plane Hall currents produces a non-vanishing Lorentz force in the z -direction (say, LF_z). Its direction within the current sheet changes from positive to negative when the sheet alters its orientation from the y - to the x -direction (see Figs. 3(d), (i)). The out-of-plane plasma flow (V_z) inside the current sheet also changes its direction (see Figs. 3(e), (j)). The directional similarities between LF_z and V_z are also present along the separatrices (see Fig. 3). Moreover, there are complex configurations of in-plane currents in the outflow regions which produce weaker inverse LF_z and V_z there (see Fig. 3).

To further ensure occurrence of the oscillatory reconnection, we examine whether the out-of-plane electric field, i.e., E_z possesses any oscillation or not at the primary location of the magnetic null, i.e., at $(x, y) = [0, 0]$ cm while keeping I_0 fixed at 1.98 kA. Basically, we calculate $E_z = -(V_x B_y - V_y B_x) + J_z / \sigma$. Here, V_x and V_y are the x - and y -components of the plasma velocity. Similarly, B_x and B_y are the x - and y -components of the magnetic field. σ is the conductivity. We find that the diffusive part of E_z , i.e., J_z / σ is much higher than the conductive part at the location of measurement (see dashed and dotted curves in Fig. 4). More importantly, we find that both diffusive and conductive parts of E_z

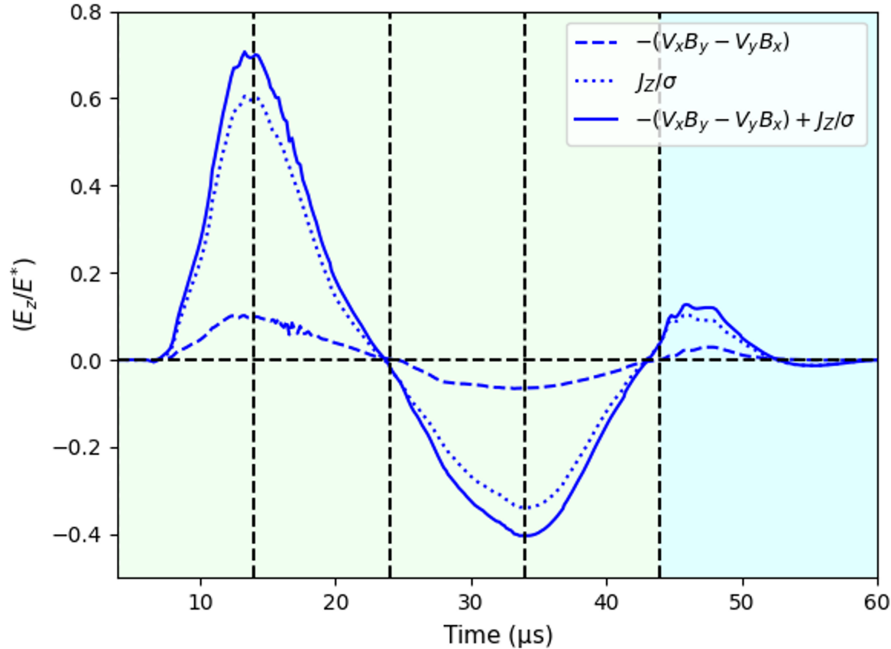


Figure 4. Oscillations in the out-of-plane electric field, i.e., E_z at $(x, y) = [0, 0]$ cm, i.e., at the primary location of the magnetic null for $I_0 = 1.98$ kA. The conductive, diffusive and total E_z are shown as dashed, dotted and solid blue curves respectively. Vertical black dashed lines denote $13.9 \mu\text{s}$, $24 \mu\text{s}$, $34 \mu\text{s}$ and $44 \mu\text{s}$, as in Fig. 1(b).

oscillate and change their direction with a reversal of the direction of the driving current (see Fig. 4). Therefore, we confirm that oscillatory reconnection is taking place at the location of magnetic null. Moreover, this oscillation in E_z is indicative of the variation in energy conversion rate with time.

3.2. Temporal Evolution of J_z , P_T and V_z at the Primary Null Location and its Dependence on I_0

Increasing the amplitude I_0 of the imposed currents produces a stronger perturbation in the magnetic field and results in more intense fast-mode waves (see Fig. 1(c)) that perturb the magnetic null to form a current sheet. The oscillatory reconnection remains similar, with a current sheet initially forming in the y -direction followed by one in the x -direction. We examine how J_z , P_T , and V_z change within the current sheet and its surroundings if we change I_0 (see Fig. 5(a) (Multimedia available online)). The magnitude of J_z within the current sheet increases with an increase in I_0 (see the top row of Fig. 5(a)). J_z within the current sheet in the absence of driving currents follows the same trend (see the animation associated with Fig. 5(a)). To have a more quantitative comparison, we calculate the change in J_z with time at the origin $(x, y) = [0, 0]$ cm between $3.9 \mu\text{s}$ and $60 \mu\text{s}$. Irrespective of I_0 , J_z begins to accumulate around $7.6 \mu\text{s}$ at the null location, and, after that, it keeps on increasing. The rate of increase of J_z is found to be higher for higher I_0 (see Fig. 5(b)). For comparatively lower values of I_0 , J_z attains a peak around $13.9 \mu\text{s}$, i.e., the time when sinusoidal driving currents reach their peak (denoted by the first vertical black dashed line in Fig. 5(b)). However, as I_0 is increased, the peaks in J_z are attained at earlier times (see Fig. 5(b)). This may indicate that the dynamics are being driven by forces generated within the simulation domain rather than just responding directly to the boundary forcing.

In all of the cases, J_z reaches zero around $24 \mu\text{s}$ and thereafter reverses its direction irrespective of the magnitude of I_0 . This time of reversal for J_z is similar to the time of reversal of the driving alternating current (denoted by the second vertical black dashed line in Fig. 5(b)). In comparison to the first phase with a y -directed current sheet, the magnitude of J_z increases with a shallower slope for all I_0 in the second phase with the x -directed current sheet and attains lower magnitudes (see Fig. 5(b)). However, slopes of change in J_z are definitely higher in the case of higher I_0 in both phases (see Fig. 5(b)). We do not even find proper dips in J_z for any of the I_0 around $34 \mu\text{s}$, i.e., the time when the driving current attains its dip (denoted by the third vertical black dashed line in Fig. 5(b)). Eventually, the magnitude of J_z again decreases and reaches zero at $44 \mu\text{s}$ for lower I_0 (denoted by the fourth vertical black dashed line in Fig. 5(b)). Interestingly, J_z reverses its direction even before $44 \mu\text{s}$ for higher I_0 . The persistence of nonzero values

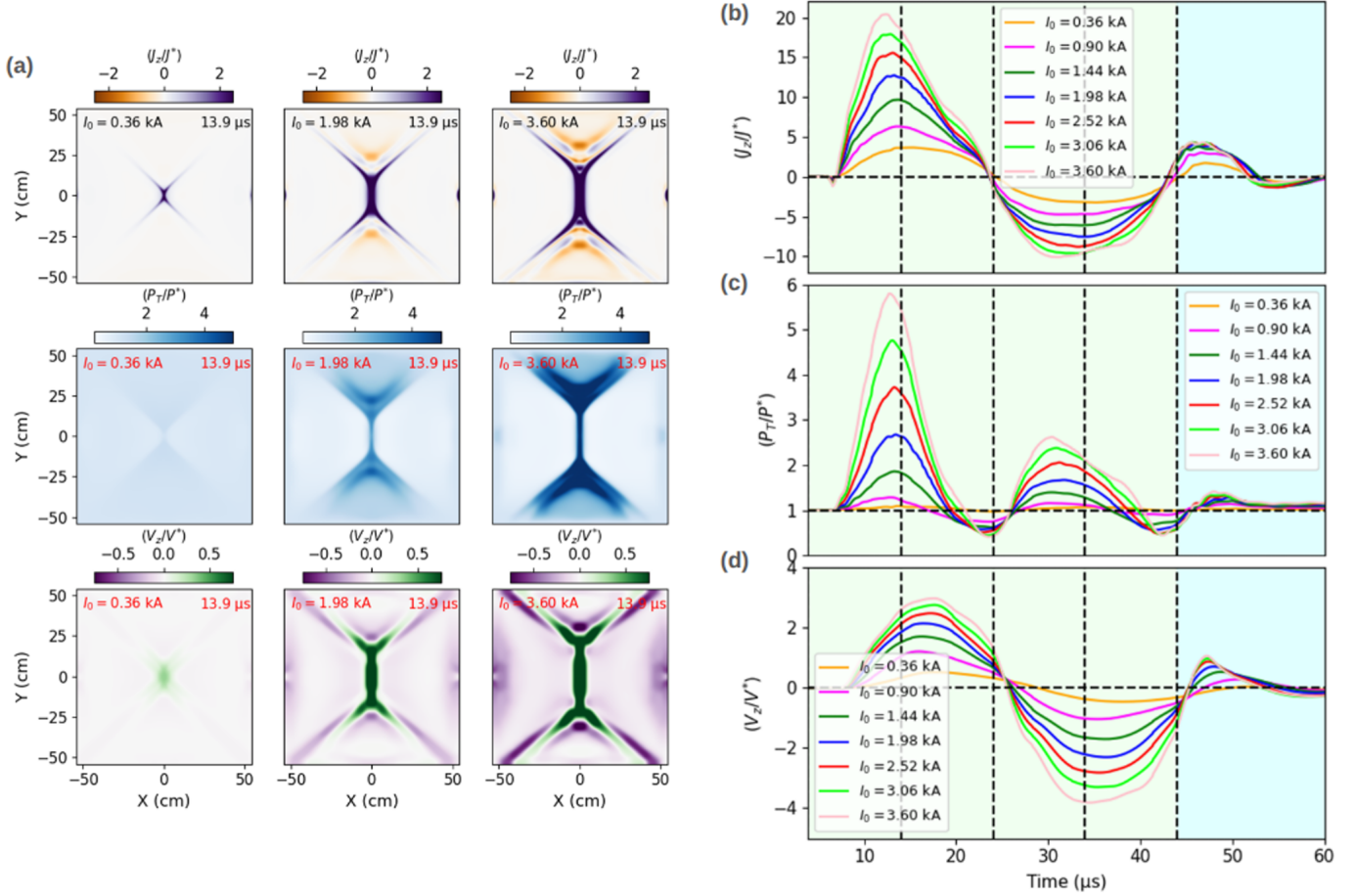


Figure 5. (a) J_z , P_T , and V_z maps at $13.9 \mu\text{s}$ for imposed alternating currents of three different amplitudes (0.36 kA, 1.98 kA and 3.60 kA) (top to bottom). The evolutions of J_z , P_T , and V_z from 7.8 to $60 \mu\text{s}$ for all three amplitudes are shown in Fig5a.mp4 (Multimedia available online). (b) The time-variation in J_z at the magnetic null $(x,y) = [0,0]$ cm. Vertical black dashed lines correspond to $13.9 \mu\text{s}$, $24 \mu\text{s}$, $34 \mu\text{s}$ and $44 \mu\text{s}$, as in Fig. 1(b) and in Fig. 4. (c) Variation in P_T with time at the same location. (d) Variation in V_z at the same location with time. Vertical black dashed lines in (c) and (d) are the same as in (b).

of J_z after the driving current is switched off is evident from the profiles of J_z in the cyan-shaded region of Fig. 5(b). J_z undergoes another oscillation in direction before declining to zero around $60 \mu\text{s}$. After the external driving is switched off, the profiles of J_z for I_0 of 0.36 kA and 0.90 kA have lower magnitudes than for higher values of I_0 . As discussed before, the contribution of the diffusive part, i.e., J_z/σ is higher to the total E_z . Therefore, the dependence of the temporal variation of J_z on I_0 is indicative of how the value of I_0 can change the features of oscillatory E_z .

Next, we examine how the magnitude of I_0 affects the temporal variation of P_T at $(x,y) = [0,0]$ cm. From the colormaps of P_T in Fig. 5(a), it is evident that an increase in I_0 increases P_T within the current sheet, along the separatrices and also in the outflow regions. At $(x,y) = [0,0]$ cm, P_T starts to increase almost around $7.6 \mu\text{s}$ irrespective of I_0 , similar to J_z . As for J_z in Fig. 5(b), the slope of increase of P_T is higher for higher I_0 . Moreover, the first peaks in P_T are also attained at earlier times than in $13.9 \mu\text{s}$ for higher I_0 (see Fig. 5(c)). After the peaks, P_T at $(x,y) = [0,0]$ cm falls to its initial background value even before the driving current vanishes during its reversal (see Fig. 5(c)). At times close to the reversal of the driving current, P_T decreases to values even smaller than its initial value. Afterwards, during the increase of the driving current in the opposite direction, P_T increases again up to roughly three times its initial value for $I_0 = 3.60 \text{ kA}$. In general, the peaks in this second phase of reconnection are much smaller than those in the first phase. Similar to the first phase, P_T decreases to its initial background value before the driving current is switched off at $44 \mu\text{s}$ for all I_0 . In fact, as time advances, the value of P_T first decreases beyond its initial value and then increases to reach near its initial value at times close to $44 \mu\text{s}$. Later, it increases again beyond its initial value before eventually reaching an equilibrium around $60 \mu\text{s}$. In general, an increase in amplitude of the driving current,

I_0 , raises the magnitude of P_T at each time (see Fig. 5(c)). In J_z , we notice one cycle of damped oscillation with a pair of peaks in opposite directions after the driving current has been switched off. However, we do not see two clear peaks in P_T .

From the spatial distribution of V_z for $I_0 = 0.36$ kA, 1.98 kA and 3.60 kA at $13.9 \mu\text{s}$, we find that V_z increases with an increase of I_0 (see Fig. 5(a)). Just like V_z and P_T at $(x,y) = [0,0]$ cm, we find that V_z starts to increase from $7.6 \mu\text{s}$. However, unlike J_z and P_T , the first peak in V_z is attained later than $13.9 \mu\text{s}$ for all values of I_0 (denoted by the first black dashed vertical line in Fig. 5(d)). Thus, there is a time lag for V_z in comparison to J_z and P_T . Furthermore, the peaks in V_z are not attained at earlier times for higher I_0 than those for lower I_0 . Following the initial time lag, V_z reaches zero at a time later than $24 \mu\text{s}$. Also, in contrast to J_z and P_T , for higher values of I_0 (i.e., for $I_0 = 2.52$ kA, 3.06 kA and 3.60 kA), the magnitude of V_z during the second stage of reconnection is larger than during the first stage with a y -directed current sheet (see Fig. 5(d)). However, in general, similar to J_z and P_T , the magnitude of V_z at $(x,y) = [0,0]$ cm increases with I_0 in both the first and second stage (see Fig. 5(d)). After the driving current is switched off, V_z undergoes a one cycle damped oscillation before vanishing at around $60 \mu\text{s}$. In these late stages, while the profiles of J_z and P_T tend to overlap (see profiles in cyan shaded regions in Figs. 5(b)-(c)), the profiles of V_z are more separate (see Fig. 5(d)).

4. DISCUSSION AND CONCLUSION

We have simulated oscillatory reconnection driven by alternating current-induced fast magnetoacoustic waves in laboratory plasma conditions. The mutually beneficial coexistence of reconnection and waves is important in the solar corona where the waves can drive reconnection and waves can be generated by reconnection (e.g., Mondal et al. 2024; Srivastava et al. 2025). The present study indicates that such a symbiosis of waves and reconnection may be relevant and significant also at the laboratory scales. We find that oscillatory reconnection can also take place in the absence of Hall effects. However, the introduction of the Hall effect generates additional features such as in-plane Hall currents, quadrupolar magnetic fields and plasma flows in the out-of-plane direction. Furthermore, strong reconnection plasma outflows generates inverse Hall currents in the outflow regions which lead to more complex configurations of B_z . All of these features are present in a laboratory experiment that studies fast wave-driven formation of a current sheet by collapse of a magnetic null (e.g., Frank & Savinov 2024).

We measure the variation in time of physical variables such as J_z , P_T and V_z at the magnetic null location for seven amplitudes of the driving current from 0.36 kA to 3.60 kA. We find that an increase in I_0 raises the values of J_z , P_T and V_z which possess nearly sinusoidal trends up to $44 \mu\text{s}$. However, V_z possesses a time-lag compared with the driving current, whereas J_z and P_T peak almost at the same time as the driving current or even slightly earlier. The higher mass of ions compared with electrons implies smaller accelerations for the ions (e.g., Mandt et al. 1994; Huba 1995; Rogers et al. 2001), which produces the time-lag in V_z . Thus, the bulk plasma possesses a finite response-time to the Hall-modified magnetic stresses.

Moreover, J_z and P_T attain higher peak values in the first stage of reconnection with a y -directed current sheet. In contrast, V_z attains higher values in the second stage for higher values of I_0 . Actually, in the initial stage, the collapse of the null is driven in the absence of prior Hall currents. Therefore, the entire wave energy is available to distort the null and thin the current sheet. As time advances, the presence of the y -directed current sheet breaks the initial symmetry, which in turn accelerates the decoupling of ions and electrons (e.g., Mandt et al. 1994; Huba 1995; Rogers et al. 2001). Hence, the Hall effects gradually start to become more dominant and to modify the background conditions and introduce dispersive effects. Therefore, the x -directed current sheet tends to possess a lower current J_z , while J_z and P_T attain lower values in the second phase than in the initial phase. The ions are accelerated at a slower rate during first-stage of reconnection within the y -directed current sheet (e.g., Mandt et al. 1994; Huba 1995; Rogers et al. 2001), but, during the second phase, V_z attains higher peaks for higher I_0 .

Oscillatory reconnection has been studied extensively under solar coronal conditions using resistive MHD simulations in 2D (e.g., Craig & McClymont 1991; McLaughlin et al. 2009, 2012; Karampelas et al. 2023) as well as in 3D (e.g., Thurgood et al. 2017) in the absence of Hall physics. From these studies, it has been found that, if the null is perturbed by a single fast wave-like pulse, oscillatory reconnection can continue for multiple cycles, either due to the reflective nature of the boundaries (e.g., Craig & McClymont 1991) or even in the absence of such reflection (e.g., McLaughlin et al. 2009). Specifically, it has been shown that the period of oscillatory reconnection decreases with an increase in the amplitude of an aperiodic velocity driver (e.g., McLaughlin et al. 2009). Later, it was also reported that the period of oscillatory reconnection is inversely proportional to the background magnetic field and the square root of J

the initial plasma pressure (e.g., [Karampelas et al. 2023](#)). In present study, we have imposed fast waves continuously at the magnetic null from 4 μs to 44 μs . We find that the current sheet changes its orientation only once. So, the system behaves nearly in accordance with the driving current until it is switched off. After 44 μs , the system possesses a damped oscillatory behaviour in which the current sheet changes its orientation before reaching quasi-equilibrium. This oscillatory behaviour is due to the reflective nature of the boundaries (e.g., [Craig & McClymont 1991](#); [Karampelas et al. 2022](#)).

Now, in solar coronal conditions, oscillatory reconnection has been found to continue for multiple cycles (e.g., [Craig & McClymont 1991](#); [McLaughlin et al. 2009](#)). However, if the Lundquist number S is less than 10^4 , the perturbation of a magnetic null will decay in less than one oscillation time (e.g., [Craig & McClymont 1991](#)). In general, it has been reported that, if the oscillatory reconnection is due to reflections from the boundaries, the time-scale for the oscillation is $\tau_{osc} = 2 \ln S \times R/v_A$ s, where R is the distance of the boundary from the position of the null and v_A is the Alfvén speed at the boundary (e.g., [Craig & McClymont 1991](#)). The oscillation will decay over a time-scale given by $\tau_{decay} = (2/\pi^2)(\ln S)^2 \times R/v_A$ s. In the present case, we have $R = 54$ cm, and $v_A = 55 \times 10^6$ cm.s⁻¹. The numerical magnetic diffusivity is $\eta_{numerical} = \delta x \times v_A$, where δx is the smallest cell size. Since the reconnection dynamics is taking place symmetrically about the centre of the domain, the system size, say, l can be considered to be the distance from the centre to the boundaries, namely, $l = R = 54$ cm. Hence, the Lundquist number S can be estimated to be 160. This makes τ_{osc} and τ_{decay} to be around 9.8 μs and 5 μs , respectively. From the estimated profiles of J_z , P_T and V_z in the absence of a driving current, we can see that the oscillation decays even before completing one oscillation. Thus, the late-stage behaviour in our simulation agrees qualitatively with what is expected for a plasma system with low Lundquist number. In future, it would be interesting to study the effects of changes in the initial background plasma density, temperature, magnetic field on the dynamics, as well as the effect of an increase in spatial resolution with an accompanying increase in effective Lundquist number. Carrying out a laboratory experiment on this scenario, as well as a fully kinetic simulation, would be invaluable.

ACKNOWLEDGMENTS

The authors are thankful to the anonymous reviewers for their valuable constructive remarks which have been very helpful in improving the manuscript. The authors appreciate the user-friendly, flexible framework of open source MPI-AMRVAC 3.0 which is helpful to perform this simulation in laboratory scales using Hall-MHD formalism. S.M. acknowledges the financial support provided by the Prime Minister’s Research Fellowship (PMRF) of India. A.K.S would like to acknowledge the ISRO grant(DS/2B-13012(2)/26/2022-Sec.2) for the support of his scientific research.

REFERENCES

- Baty, H. 2000, *A&A*, 353, 1074
- Birn, J., Drake, J. F., Shay, M. A., et al. 2001, *J. Geophys. Res.*, 106, 3715, doi: [10.1029/1999JA900449](#)
- Browning, P. K., Gordovskyy, M., Schiavo, L. A. C. A., & Stewart, J. 2024, *Fundamental Plasma Physics*, 10, 100049, doi: [10.1016/j.fpp.2024.100049](#)
- Craig, I., & McClymont, A. 1991, *Astrophys. J.*, 371, L41, doi: [10.1086/185997](#)
- Drake, J. F., Shay, M. A., & Swisdak, M. 2008, *Physics of Plasmas*, 15, 042306, doi: [10.1063/1.2901194](#)
- Drake, J. F., Antiochos, S. K., Bale, S. D., et al. 2025, *SSRv*, 221, 27, doi: [10.1007/s11214-025-01153-x](#)
- Egedal, J. 2021, Exploring 3D Collisionless Magnetic Reconnection in the Laboratory, NASA Proposal ID. 21-HTIDS21-0003
- Fiksel, G., Fox, W., Bhattacharjee, A., et al. 2014, *PhRvL*, 113, 105003, doi: [10.1103/PhysRevLett.113.105003](#)
- Fox, W., Bhattacharjee, A., & Germaschewski, K. 2011, in 2010 NASA Laboratory Astrophysics Workshop, C45
- Fox, W., Schaeffer, D., Fiksel, G., et al. 2022, in APS Meeting Abstracts, Vol. 2022, APS Division of Plasma Physics Meeting Abstracts, CM09.005
- Frank, A. G., & Savinov, S. A. 2024, *Symmetry*, 16, 103, doi: [10.3390/sym16010103](#)
- Gershman, D. J., Fuselier, S. A., Cohen, I. J., et al. 2024, *SSRv*, 220, 7, doi: [10.1007/s11214-023-01017-2](#)
- Goedbloed, J. P. H., & Poedts, S. 2004, *Principles of Magnetohydrodynamics*
- Hare, J. D., Suttle, L., Lebedev, S. V., et al. 2017, *PhRvL*, 118, 085001, doi: [10.1103/PhysRevLett.118.085001](#)
- Harten, A. 1983, *Journal of Computational Physics*, 49, 357, doi: [10.1016/0021-9991\(83\)90136-5](#)
- Hesse, M., & Cassak, P. A. 2020, *Journal of Geophysical Research (Space Physics)*, 125, e25935, doi: [10.1029/2018JA025935](#)

- Huba, J. D. 1995, *Physics of Plasmas*, 2, 2504, doi: [10.1063/1.871212](https://doi.org/10.1063/1.871212)
- Huba, J. D. 2003, in *Space Simulations*, ed. M. Scholer, C. Dum, & J. Büchner (New York: Springer), 170–197
- Huba, J. D., & Rudakov, L. I. 2002, *Phys. Plasmas*, 9, 4435
- Huba, J. D., & Rudakov, L. I. 2003, *Physics of Plasmas*, 10, 3139, doi: [10.1063/1.1582474](https://doi.org/10.1063/1.1582474)
- Karampelas, K., McLaughlin, J. A., Botha, G. J. J., & Régnier, S. 2022, *ApJ*, 925, 195, doi: [10.3847/1538-4357/ac3b53](https://doi.org/10.3847/1538-4357/ac3b53)
- . 2023, *ApJ*, 943, 131, doi: [10.3847/1538-4357/acac90](https://doi.org/10.3847/1538-4357/acac90)
- Keppens, R., Popescu Braileanu, B., Zhou, Y., et al. 2023, *A&A*, 673, A66, doi: [10.1051/0004-6361/202245359](https://doi.org/10.1051/0004-6361/202245359)
- Knoll, D. A., & Chacón, L. 2006, *PhRvL*, 96, 135001, doi: [10.1103/PhysRevLett.96.135001](https://doi.org/10.1103/PhysRevLett.96.135001)
- Leroy, M. H. J., & Keppens, R. 2017, *Physics of Plasmas*, 24, 012906, doi: [10.1063/1.4974758](https://doi.org/10.1063/1.4974758)
- Malakit, K., Cassak, P. A., Shay, M. A., & Drake, J. F. 2009, *Geophys. Res. Lett.*, 36, L07107, doi: [10.1029/2009GL037538](https://doi.org/10.1029/2009GL037538)
- Mandt, M. E., Denton, R. E., & Drake, J. F. 1994, *Geophys. Res. Lett.*, 21, 73, doi: [10.1029/93GL03382](https://doi.org/10.1029/93GL03382)
- McLaughlin, J. A., De Moortel, I., Hood, A. W., & Brady, C. S. 2009, *A&A*, 493, 227, doi: [10.1051/0004-6361:200810465](https://doi.org/10.1051/0004-6361:200810465)
- McLaughlin, J. A., Thurgood, J. O., & MacTaggart, D. 2012, *A&A*, 548, A98, doi: [10.1051/0004-6361/201220234](https://doi.org/10.1051/0004-6361/201220234)
- Mondal, S., Srivastava, A. K., Pontin, D. I., et al. 2024, *ApJ*, 977, 235, doi: [10.3847/1538-4357/ad9022](https://doi.org/10.3847/1538-4357/ad9022)
- Moreno-Insertis, F., Hansteen, V. H., & Nóbrega-Siverio, D. 2025, arXiv e-prints, arXiv:2510.19993, doi: [10.48550/arXiv.2510.19993](https://doi.org/10.48550/arXiv.2510.19993)
- Nakamura, R., Burch, J. L., Birn, J., et al. 2025, *SSRv*, 221, 17, doi: [10.1007/s11214-025-01143-z](https://doi.org/10.1007/s11214-025-01143-z)
- Olson, J., Egedal, J., Greess, S., et al. 2016, *PhRvL*, 116, 255001, doi: [10.1103/PhysRevLett.116.255001](https://doi.org/10.1103/PhysRevLett.116.255001)
- Pontin, D. I., & Priest, E. R. 2022, *Living Reviews in Solar Physics*, 19, 1, doi: [10.1007/s41116-022-00032-9](https://doi.org/10.1007/s41116-022-00032-9)
- Pontin, D. I., Wyper, P. F., & Priest, E. R. 2024, in *Magnetohydrodynamic Processes in Solar Plasmas*, ed. A. K. Srivastava, M. Goossens, & I. Arregui, 345–414, doi: [10.1016/B978-0-32-395664-2.00014-1](https://doi.org/10.1016/B978-0-32-395664-2.00014-1)
- Priest, E. 2014, *Magnetohydrodynamics of the Sun*, doi: [10.1017/CBO9781139020732](https://doi.org/10.1017/CBO9781139020732)
- Richter, M. M., Muñoz, P. A., & Spanier, F. 2025, *Physics of Plasmas*, 32, 093904, doi: [10.1063/5.0268535](https://doi.org/10.1063/5.0268535)
- Rogers, B. N., Denton, R. E., Drake, J. F., & Shay, M. A. 2001, *PhRvL*, 87, 195004, doi: [10.1103/PhysRevLett.87.195004](https://doi.org/10.1103/PhysRevLett.87.195004)
- Sakai, J., Tajima, T., & Brunel, F. 1984, *SoPh*, 91, 103, doi: [10.1007/BF00213617](https://doi.org/10.1007/BF00213617)
- Shay, M., Adhikari, S., Beesho, N., et al. 2025, *SSRv*, 221, 81, doi: [10.1007/s11214-025-01210-5](https://doi.org/10.1007/s11214-025-01210-5)
- Shay, M. A., Drake, J. F., Rogers, B. N., & Denton, R. E. 2001, *J. Geophys. Res.*, 106, 3759, doi: [10.1029/1999JA001007](https://doi.org/10.1029/1999JA001007)
- Srivastava, A. K., Mishra, S. K., Jelínek, P., et al. 2019, *ApJ*, 887, 137, doi: [10.3847/1538-4357/ab4a0c](https://doi.org/10.3847/1538-4357/ab4a0c)
- Srivastava, A. K., Mondal, S., Priest, E. R., et al. 2025, *ApJ*, 984, 36, doi: [10.3847/1538-4357/adc379](https://doi.org/10.3847/1538-4357/adc379)
- Stanier, A., Daughton, W., Simakov, A. N., et al. 2017, *Physics of Plasmas*, 24, 022124, doi: [10.1063/1.4976712](https://doi.org/10.1063/1.4976712)
- Thurgood, J. O., Pontin, D. I., & McLaughlin, J. A. 2017, *ApJ*, 844, 2, doi: [10.3847/1538-4357/aa79fa](https://doi.org/10.3847/1538-4357/aa79fa)
- Uzdensky, D. A., & Kulsrud, R. M. 2006, *Physics of Plasmas*, 13, 062305, doi: [10.1063/1.2209627](https://doi.org/10.1063/1.2209627)
- van Leer, B. 1979, *Journal of Computational Physics*, 32, 101, doi: [10.1016/0021-9991\(79\)90145-1](https://doi.org/10.1016/0021-9991(79)90145-1)
- Vekstein, G. 2017, *Journal of Plasma Physics*, 83, 205830501, doi: [10.1017/S0022377817000782](https://doi.org/10.1017/S0022377817000782)
- Yamada, M., Ji, H., Kulsrud, R., et al. 2005, in *American Institute of Physics Conference Series*, Vol. 784, *Magnetic Fields in the Universe: From Laboratory and Stars to Primordial Structures.*, ed. E. M. de Gouveia dal Pino, G. Lugones, & A. Lazarian (AIP), 27–41, doi: [10.1063/1.2077169](https://doi.org/10.1063/1.2077169)
- Yamada, M., Kulsrud, R., & Ji, H. 2010, *Reviews of Modern Physics*, 82, 603, doi: [10.1103/RevModPhys.82.603](https://doi.org/10.1103/RevModPhys.82.603)
- Yamada, M., Yoo, J., Jara-Almonte, J., et al. 2014, *Nature Communications*, 5, 4774, doi: [10.1038/ncomms5774](https://doi.org/10.1038/ncomms5774)
- Yamada, M., Yoo, J., & Myers, C. E. 2016, *Physics of Plasmas*, 23, 055402, doi: [10.1063/1.4948721](https://doi.org/10.1063/1.4948721)
- Yamada, M., Ji, H., Hsu, S., et al. 1997, *Physics of Plasmas*, 4, 1936, doi: [10.1063/1.872336](https://doi.org/10.1063/1.872336)